

Active RIS vs. Passive RIS: Which Will Prevail in 6G?

Zijian Zhang, Linglong Dai, *Fellow, IEEE*, Xibi Chen, Changhao Liu, Fan Yang, *Fellow, IEEE*, Robert Schober, *Fellow, IEEE*, and H. Vincent Poor, *Life Fellow, IEEE*

Abstract—As a revolutionary paradigm for controlling wireless channels, reconfigurable intelligent surface (RIS) has emerged as a candidate technology for future 6G networks. However, due to the “multiplicative fading” effect, the existing passive RISs only achieve a negligible capacity gain in many scenarios with strong direct links. In this paper, the concept of active RISs is proposed to overcome this fundamental limitation. Unlike the existing passive RISs that reflect signals without amplification, active RISs can amplify the reflected signals actively through integrating amplifiers into their elements. To characterize the signal amplification and incorporate the noise introduced by active components, we develop a signal model for active RISs, which is validated through the experimental measurements on a fabricated active RIS element. Based on the developed signal model, we further analyze the asymptotic performance of active RISs to reveal its notable capacity gain for wireless communications. Finally, we formulate the sum-rate maximization problem for an active RIS aided multiple-input multiple-output (MIMO) system and a joint transmit beamforming and reflect precoding algorithm is proposed to solve this problem. Simulation results show that, in a typical wireless system, the existing passive RISs can realize only a negligible sum-rate gain of 3%, while the proposed active RISs can achieve a significant sum-rate gain of 108%, thus overcoming the “multiplicative fading” effect.

Index Terms—Reconfigurable intelligent surface (RIS), beamforming, active RIS, signal model.

I. INTRODUCTION

As wireless communications have advanced from the first generation (1G) to 5G, the system capacity has been significantly increased by improving the transceiver designs, while the wireless channels have been usually considered to be uncontrollable. Recently, due to the advances in metamaterials, reconfigurable intelligent surfaces (RISs) have been proposed [1]–[4] for the purpose of intelligently controlling wireless channels for improved communication performances. Specifically, an RIS is an array composed of a very large number of passive elements that reflects electromagnetic signals in a desired manner so as to reconfigure the propagation

properties of the wireless environment [5]. Thanks to their high array gain, low cost, low power, and low noise [5]–[7], RISs promise to improve channel capacity [8], extend coverage [9], and save power [10] in future 6G networks. Additionally, RISs are also projected to have other applications such as in WiFi [11], precision measurement [12], and navigation [13].

As an important advantage of RIS, the negligible noise introduced by passive RISs enables a “square-law” array gain. Specifically, the array gain of an N -element RIS is proportional to N^2 , which is N times larger than that achievable by standard massive multiple-input multiple-output (MIMO) systems [5]. Benefiting from this advantage, RISs are expected to introduce significant capacity gains in wireless systems [8]. However, in practice, these capacity gains are typically only observed in communication scenarios where the direct link between transmitter and receiver is completely blocked or very weak [8]–[10], [14]–[16]. By contrast, in many scenarios where the direct link is not weak, common RISs can achieve only negligible capacity gains [17]. The reason behind this phenomenon is the “multiplicative fading” effect introduced by RISs, i.e., the equivalent path loss of the transmitter-RIS-receiver link is the product (instead of the sum) of the path losses of the transmitter-RIS link and RIS-receiver link, which is usually thousands of times larger than that of the direct link [17]. As a result, the “multiplicative fading” effect makes it almost impossible for passive RISs to achieve noticeable capacity gains in many wireless environments. Many existing works on RISs have bypassed this effect by only considering scenarios with very poor direct links [8]–[10], [14]–[16]. Therefore, to advance the practicability of RISs in future 6G wireless networks, a critical issue for RISs to be addressed is: *How to break the fundamental performance bottleneck caused by the “multiplicative fading” effect?*

To overcome the fundamental physical limitation imposed by the “multiplicative fading” effect, the new concept of active RIS is proposed in this paper. Specifically, our contributions are summarized as follows:

- To break the fundamental performance bottleneck of conventional passive RISs, we propose the concept of *active* RISs to overcome the “multiplicative fading” effect. Different from the existing *passive* RISs that passively reflect signals without amplification, the key feature of active RISs is their capability of actively reflecting signals with amplification at the expense of additional power consumption, which can be realized by integrating reflection-type amplifiers into their reflecting elements.
- We develop a new signal model for the proposed active RISs, which characterizes the amplification of the incident signal and incorporates the non-negligible thermal

Z. Zhang, L. Dai, X. Chen, C. Liu, and F. Yang are with the Department of Electronic Engineering as well as the Beijing National Research Center for Information Science and Technology (BNRist), Tsinghua University, Beijing 100084, China (e-mails: zhangzij15@mails.tsinghua.edu.cn, daill@tsinghua.edu.cn, cxb17@mails.tsinghua.edu.cn, liuch17@mails.tsinghua.edu.cn, fan_yang@tsinghua.edu.cn).

R. Schober is with the Institute for Digital Communications at Friedrich-Alexander University Erlangen-Nürnberg (FAU) (e-mail: robert.schober@fau.de).

H. V. Poor is with the Department of Electrical and Computer Engineering, Princeton University, USA (e-mail: poor@princeton.edu).

This work was supported in part by the National Key Research and Development Program of China (Grant No. 2020YFB1807201), in part by the National Natural Science Foundation of China (Grant No. 62031019), and in part by the U.S. National Science Foundation under Grants CCF-0939370 and CCF-1908308.

noise introduced by the active elements. For verification, an active RIS element was designed and fabricated to validate the developed signal model through experimental measurements. Based on the developed signal model, we further analyze the asymptotic performance of active RISs and compare it to that of the existing passive RISs, which reveals the notable capacity gain enabled by the use of active RISs.

- To evaluate the performance of active RISs in typical communication systems, we formulate a sum-rate maximization problem for an active RIS aided MIMO system. Then, a joint transmit beamforming and reflect precoding algorithm is proposed to solve this problem. Simulation results show that, in a typical wireless system, the existing passive RISs achieve only a negligible sum-rate gain of 3%, while the proposed active RISs are able to achieve a noticeable sum-rate gain of 108%, thus overcoming the “multiplicative fading” effect.

The rest of this paper is organized as follows. In Section II, the concept of active RISs is introduced, and the signal model of active RIS is developed. In Section III, the asymptotic performance of active RISs is analyzed and compared to that of the existing passive RISs. In Section IV, the sum-rate maximization problem is formulated, and the precoding design for capacity maximization is proposed to solve the formulated problem. In Section V, experimental measurements are presented to validate the developed signal model, and the numerical simulation results are provided to evaluate the performance of active RISs in typical communication systems. Finally, conclusions are drawn and future works are discussed in Section VI.

Notations: \mathbb{C} , \mathbb{R} , and \mathbb{R}_+ denote the sets of complex, real, and positive real numbers, respectively; $[\cdot]^{-1}$, $[\cdot]^T$, and $[\cdot]^H$ denote the inverse, transpose, and conjugate-transpose operations, respectively; $\|\cdot\|$ denotes the Frobenius norm of its argument; $\text{diag}(\cdot)$ denotes the diagonal matrix of its argument; $\Re\{\cdot\}$ denotes the real part of its argument; \otimes denotes the Kronecker product; $\angle[\cdot]$ denotes the angle of its complex argument; $\ln(\cdot)$ denotes the natural logarithm of its argument; $\mathcal{CN}(\boldsymbol{\mu}, \boldsymbol{\Sigma})$ denotes the complex multivariate Gaussian distribution with mean $\boldsymbol{\mu}$ and variance $\boldsymbol{\Sigma}$; \mathbf{I}_L is an $L \times L$ identity matrix, and $\mathbf{0}_L$ is an $L \times 1$ zero vector.

II. CONCEPT OF ACTIVE RIS

In this section, we propose the concept of active RISs. First, we review the existing passive RISs, and point out their fundamental physical limitation imposed by the “multiplicative fading” effect in Subsection II-A. Then, to overcome this limitation, we propose the concept of active RISs along with their hardware structure and signal model in Subsection II-B. Finally, we present the transmission model for an active RIS aided MIMO system in Subsection II-C.

A. Existing Passive RISs

The RISs widely studied in existing works are passive RISs [1]–[10]. Specifically, as shown in Fig. 1 (a), a passive RIS comprises a large number of passive elements each being able

to reflect the incident signal with a controllable phase shift. In general, each passive RIS element consists of a reflective patch terminated with an impedance-adjustable circuit for phase shifting [18]. Thanks to its passive operating mode without active radio-frequency (RF) components, a passive RIS element practically consumes zero direct-current power [18], and the introduced thermal noise is usually negligible [5]–[10]. Thereby, the signal model of an N -element passive RIS widely used in the literature is given as follows [6]

$$\mathbf{y} = \boldsymbol{\Theta}\mathbf{x}, \quad (1)$$

where $\mathbf{x} \in \mathbb{C}^N$ denotes the incident signal, $\boldsymbol{\Theta} := \text{diag}(e^{j\theta_1}, \dots, e^{j\theta_N}) \in \mathbb{C}^{N \times N}$ denotes the phase shift matrix of the RIS, and $\mathbf{y} \in \mathbb{C}^N$ denotes the signal reflected by the RIS. Note that, the impact of noise is neglected in (1). As a consequence, by properly adjusting $\boldsymbol{\Theta}$ to manipulate the N signals reflected by the N RIS elements to coherently add with the same phase at the receiver, a high array gain proportional to N^2 can be achieved. This is expected to significantly increase the receiver signal-to-noise ratio (SNR) [5]–[7], which is one of the key reasons for why RISs have attracted so much research interest recently [8]–[16].

Unfortunately, in practice, this expected high capacity gain often cannot be achieved in many communication scenarios, where the direct link between the transmitter and the receiver is not weak. The reason for this result is the “multiplicative fading” effect introduced by passive RISs. Specifically, the equivalent path loss of the transmitter-RIS-receiver reflection link is the product (instead of the sum) of the path losses of the transmitter-RIS link and RIS-receiver link, and therefore, it is thousands of times larger than that of the unobstructed direct link. Thereby, for an RIS to realize a noticeable capacity gain, thousands of RIS elements are required to compensate for this extremely large path loss.

Remark 1: To see the above fact, let us consider a single-input single-output (SISO) system aided by a passive RIS with elements spacing of a half wavelength [19]. Let $d = 200$ m, $d_t = 150$ m, and $d_r = 200$ m denote the distances between transmitter and receiver, transmitter and RIS, RIS and receiver, respectively. For carrier frequencies of 5/10/20 GHz, according to the RIS “multiplicative fading” model in [17], $N = 10000/20000/40000$ RIS elements are required to make the reflection link as strong as the direct link. Due to the high signaling overhead introduced by the N pilots required for channel estimation [20] and the high complexity of $\mathcal{O}(N^2)$ for real-time beamforming [21]. Such a large number of RIS elements makes the application of passive RISs in practical wireless networks very challenging [17]. Consequently, many existing works have bypassed the “multiplicative fading” effect by only considering the scenario where the direct link is completely blocked or very weak [5]–[10], [14]–[16].

B. Proposed Active RISs

To overcome the fundamental performance bottleneck caused by the “multiplicative fading” effect of RISs, we propose the concept of active RISs as a promising solution. As shown in Fig. 1 (b), similar to the existing passive RISs, active

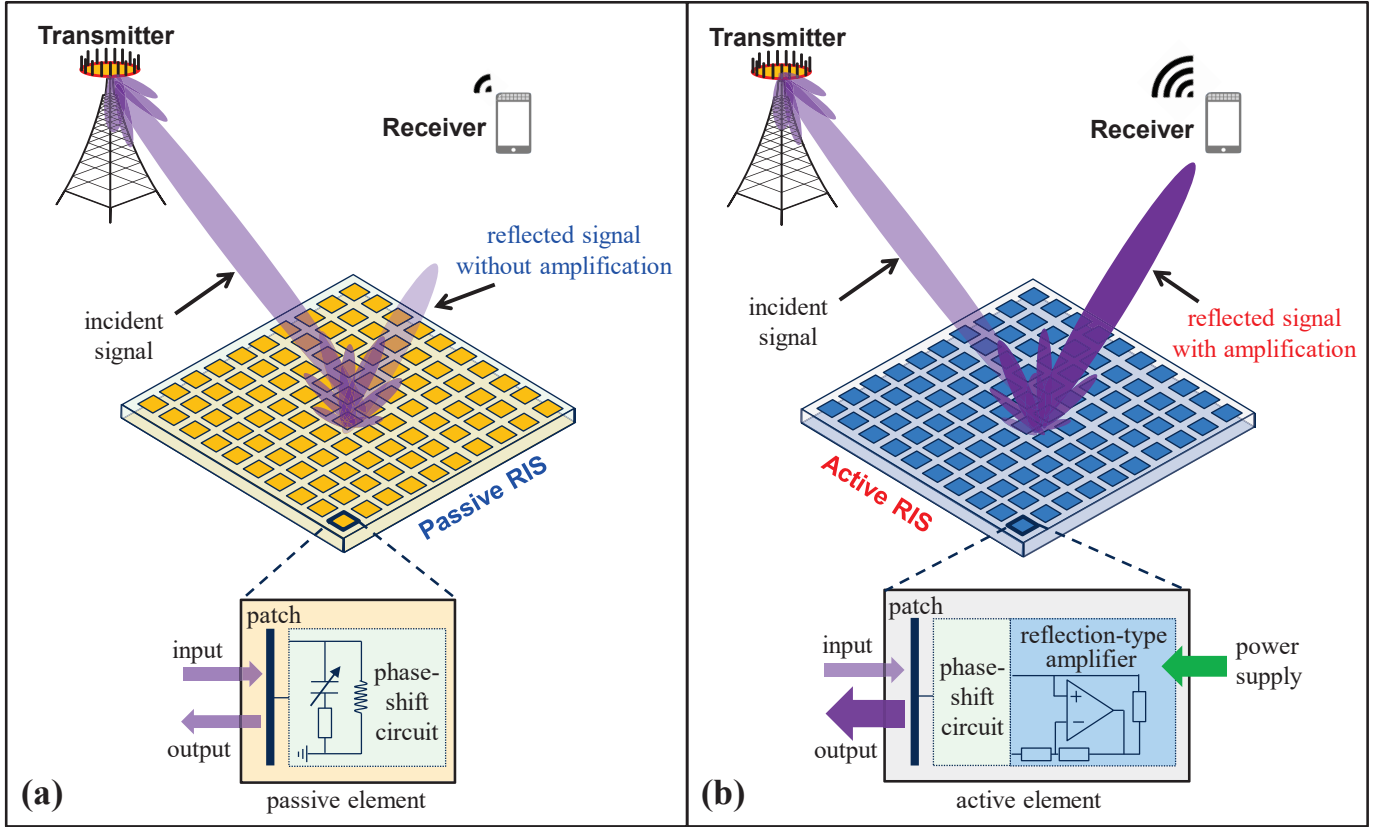


Fig. 1. Comparison between (a) the existing passive RIS and (b) the proposed active RIS.

RISs can also reflect the incident signals with reconfigurable phase shifts. Different from passive RISs that just reflect signals without amplification, active RISs can further amplify the reflected signals. To achieve this goal, the key component of an active RIS element is the additionally integrated active reflection-type amplifier, which can be realized by different existing active components, such current-inverting converters [22], asymmetric current mirrors [23], or some integrated circuits [24].¹

With the reflection-type amplifiers supported by power supplies, the reflected and amplified signal of an N -element active RIS can be modeled as follows:

$$\mathbf{y} = \underbrace{\mathbf{P}\Theta\mathbf{x}}_{\text{Desired signal}} + \underbrace{\mathbf{P}\Theta\mathbf{v}}_{\text{Dynamic noise}} + \underbrace{\mathbf{n}_s}_{\text{Static noise}}, \quad (2)$$

where $\mathbf{P} := \text{diag}(p_1, \dots, p_N) \in \mathbb{R}_+^{N \times N}$ denotes the amplification factor matrix of the active RIS, wherein each element p_n can be larger than one thanks to the integrated reflection-type amplifier. Due to the use of active components, active RISs consume additional power for amplifying the reflected signals, and the thermal noise introduced by active RIS elements cannot be neglected as is done for passive RISs. Particularly, as shown in (2), the introduced noise processes can be classified into dynamic noise and static noise [23]. Specifically, \mathbf{v} is related to the input noise and the inherent device noise of active RIS elements [23], while the static noise \mathbf{n}_s is unrelated

¹In this paper, we focus on studying reflective active RISs, while the investigation of transmissive active RISs is left for future work [25]–[27].

to \mathbf{P} and is usually negligible compared to the dynamic noise $\mathbf{P}\Theta\mathbf{v}$, which will be verified by experimental results in later Section V-A. For simplification, here we neglect \mathbf{n}_s and model \mathbf{v} as $\mathbf{v} \sim \mathcal{CN}(\mathbf{0}_N, \sigma_v^2 \mathbf{I}_N)$.

Remark 2: Note that, the proposed active RISs are fundamentally different from the RISs equipped with RF components [28]–[30] and the relays [31]. Specifically, in [28]–[30], some passive RIS elements are connected to additional active RF chains, which are used for sending pilot signals and processing baseband signals. Thus, these RIS elements have signal processing capabilities [28]–[30]. On the contrary, the proposed active RISs do not have such capabilities but only reflect and amplify the incident signals to strengthen the reflection links. Besides, although the proposed active RISs can amplify the incident signals, similar to full-duplex amplify-and-forward (FD-AF) relays, their respective hardware structures and transmission models are quite different. Specifically, an FD-AF relay is equipped with RF chains to receive the incident signal and then transmit it after amplification [31]. Due to the long delay inherent to this process, two time slots are needed to complete the transmission of one symbol, and the received signal at the receiver in a time slot actually carries two different symbols, which are transmitted by the transmitter and the FD-AF relay, respectively [31]. In this way, in order to efficiently decode the symbols, the receiver in an FD-AF relay aided system has to combine the received signals in two adjacent time slots to maximize the SNR. Thus, FD-AF relaying involves two different transmission models in two

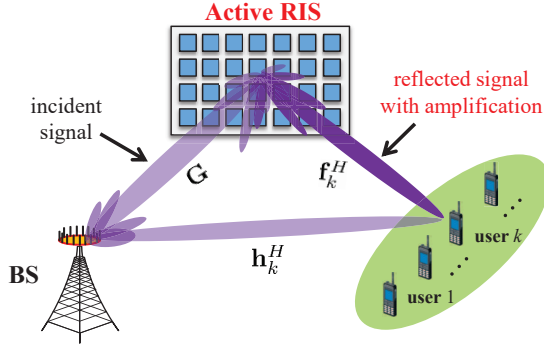


Fig. 2. An illustration of the downlink transmission in an active RIS aided MIMO system.

adjacent time slots [31, Eq. (22), Eq. (25)], while the proposed active RIS follows the name transmission model (4) in each time slot, which also leads to different achievable rates [31, Table I].

C. Active RIS Aided MIMO System

To characterize the performance gains enabled by active RISs in typical communication scenarios, we consider an active RIS aided downlink MIMO system as shown in Fig. 2, where an M -antenna base station (BS) serves K single-antenna users simultaneously with the aid of an N -element active RIS.

Let $\mathbf{s} := [s_1, \dots, s_K]^T \in \mathbb{C}^K$ denote the transmitted symbol vector for the K users with $\mathbb{E}\{\mathbf{s}\mathbf{s}^H\} = \mathbf{I}_K$. Assuming that the multi-user linear beamforming is employed at the BS for downlink transmissions, the signal reflected by the active RIS \mathbf{y} can be modeled as

$$\mathbf{y} = \mathbf{P}\mathbf{O}\mathbf{G} \sum_{j=1}^K \mathbf{w}_j s_j + \mathbf{P}\mathbf{O}\mathbf{v}, \quad (3)$$

where $\mathbf{G} \in \mathbb{C}^{N \times M}$ denotes the channels from BS to RIS and $\mathbf{w}_k \in \mathbb{C}^{M \times 1}$ denotes the BS beamforming vector for symbol s_k . Thus, according to (3), the signal $r_k \in \mathbb{C}$ received at user k can be modeled as

$$\begin{aligned} r_k &= \mathbf{h}_k^H \sum_{j=1}^K \mathbf{w}_j s_j + \mathbf{f}_k^H \mathbf{y} + z_k \\ &= \underbrace{(\mathbf{h}_k^H)}_{\text{Direct link}} + \underbrace{(\mathbf{f}_k^H \mathbf{P}\mathbf{O}\mathbf{G})}_{\text{Reflection link}} \sum_{j=1}^K \mathbf{w}_j s_j + \underbrace{(\mathbf{f}_k^H \mathbf{P}\mathbf{O}\mathbf{v})}_{\text{Noise introduced by active RIS}} + z_k \end{aligned} \quad (4)$$

where $\mathbf{h}_k^H \in \mathbb{C}^{1 \times M}$ and $\mathbf{f}_k^H \in \mathbb{C}^{1 \times N}$ denote the channels from BS to user k and those from RIS to user k , respectively; and z_k denotes the additive white Gaussian noise (AWGN) at user k with zero mean and variance σ^2 .

To theoretically illustrate how the proposed active RISs can overcome the ‘‘multiplicative fading’’ effect, based on the signal model in (2), the performance gain enabled by the use of active RISs in communications will be analyzed in the next section.

III. PERFORMANCE ANALYSIS

In this section, we analyze the performance for the proposed active RIS to reveal its notable capacity gain in theory. Firstly, the asymptotic SNR of a passive RIS aided system and that of an active RIS aided system are provided in Subsection III-A. Then, to show the superiority of active RISs, the derived asymptotic SNR for the two systems are compared in Subsection III-B.

A. Asymptotic SNR for Passive RISs and Active RISs

To reveal more insights, we first study the user’s achievable SNR in a simplified SISO scenario by setting $M = 1$ and $K = 1$, while it will be extended to a more general MIMO scenario in later Section IV. To focus on the capacity gain provided by the active RIS aided reflection link, we ignore the direct link by setting \mathbf{h}_k to zero, which is similar to [32]. For simplicity, we assume that each active RIS element has the same amplification factor ($p_n := p$ for all $n \in \{1, \dots, N\}$).

For the above communication system, we first provide the following lemma in [32] to show the asymptotic SNR for the existing passive RISs.

Lemma 1 (Asymptotic SNR for passive RISs): Assuming $\mathbf{f} \sim \mathcal{CN}(\mathbf{0}_N, \varrho_f^2 \mathbf{I}_N)$, $\mathbf{g} \sim \mathcal{CN}(\mathbf{0}_N, \varrho_g^2 \mathbf{I}_N)$ and letting $N \rightarrow \infty$, the asymptotic SNR γ_{passive} of a passive RIS aided SISO system is

$$\gamma_{\text{passive}} \rightarrow N^2 \frac{P_{\text{BS}}^{\text{max}} \pi^2 \varrho_f^2 \varrho_g^2}{16\sigma^2} \quad (5)$$

where $P_{\text{BS}}^{\text{max}}$ denotes the maximum transmit power at the BS.

Proof: Constructive proof can be found in [32]. ■

For comparisons, under the same transmission conditions, we derive the asymptotic SNR of an active RIS aided SISO system and provide the following lemma.

Lemma 2 (Asymptotic SNR for active RISs): Assuming $\mathbf{f} \sim \mathcal{CN}(\mathbf{0}_N, \varrho_f^2 \mathbf{I}_N)$, $\mathbf{g} \sim \mathcal{CN}(\mathbf{0}_N, \varrho_g^2 \mathbf{I}_N)$ and letting $N \rightarrow \infty$, the asymptotic SNR γ_{active} of an active RIS aided SISO system is

$$\gamma_{\text{active}} \rightarrow N \frac{P_{\text{BS}}^{\text{max}} P_{\text{A}}^{\text{max}} \pi^2 \varrho_f^2 \varrho_g^2}{16 \left(P_{\text{A}}^{\text{max}} \sigma_v^2 \varrho_f^2 + P_{\text{BS}}^{\text{max}} \sigma^2 \varrho_g^2 + \sigma^2 \sigma_v^2 \right)}, \quad (6)$$

where $P_{\text{A}}^{\text{max}}$ denotes the maximum reflect power at the active RIS.

Proof: Please see Appendix A. ■

To see more insights, in the next subsection, we will compare the derived asymptotic SNR for passive RISs in Lemma 1 and that for active RISs in Lemma 2 to reveal the superiority of using active RISs in wireless communications.

B. Comparisons between Passive RISs and Active RISs

We can observe from Lemma 1 and Lemma 2 that, compared to the asymptotic SNR for passive RISs γ_{passive} in (5) which is proportional to N^2 , the asymptotic SNR for active RISs γ_{active} in (6) is proportional to N due to the noises additionally introduced by the use of active components. At first glance, it seems that the SNR proportional to N^2 achieved by passive RISs γ_{passive} exceeds the SNR proportional to N achieved by

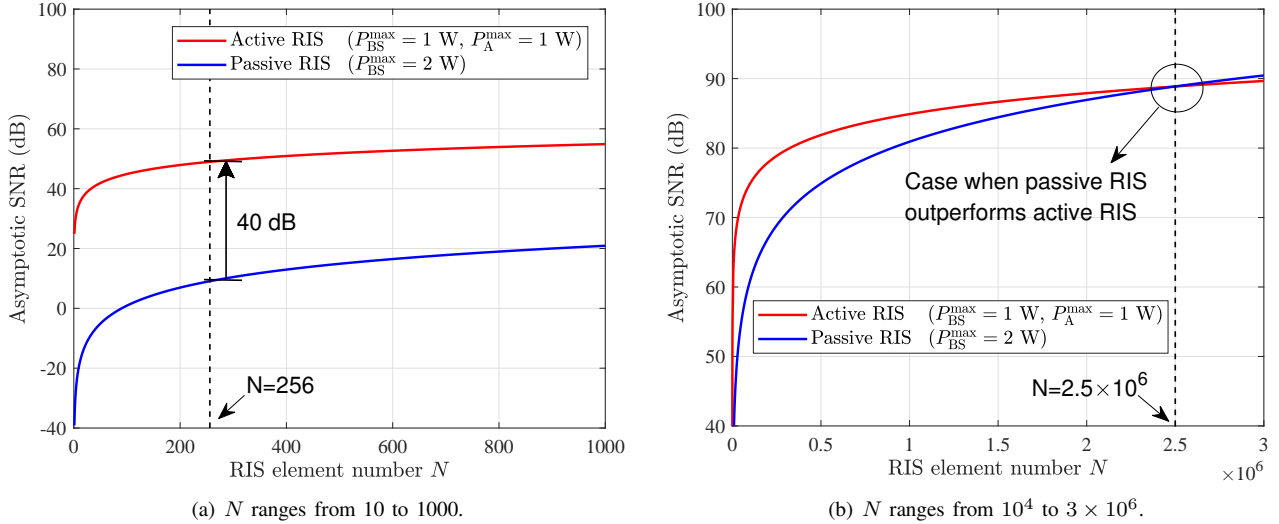


Fig. 3. The simulation results of the asymptotic SNR against the number of RIS elements N with different ranges of N .

active RISs γ_{active} . However, actually the opposite is true. The reason behind this counterintuitive behavior is that, due to the large path loss caused by the “multiplicative fading” effect and thanks to the use of reflection-type amplifiers in active RISs, only when N is unaffordably large can passive RISs outperform active RISs.

To see the above fact, let us consider two different SISO systems, which are aided by an active RIS and a passive RIS, respectively. Then, we obtain the following lemma to illustrate the unusual case when passive RISs can outperform active RISs.

Lemma 3 (Case when passive RISs outperform active RISs): Assuming the number of RIS elements N is large, the required number of elements N for passive RISs to outperform active RISs has to satisfy

$$N \geq \frac{P_{BS-A}^{\max}}{P_{BS-P}^{\max}} \frac{P_A^{\max} \sigma^2}{\left(P_A^{\max} \sigma_v^2 \varrho_f^2 + P_{BS-A}^{\max} \sigma^2 \varrho_g^2 + \sigma^2 \sigma_v^2 \right)}, \quad (7)$$

where P_{BS-A}^{\max} denotes the maximum BS transmit power in the active RIS aided system and P_{BS-P}^{\max} denotes that in the passive RIS aided system.

Proof: Please see Appendix B. ■

Consider a specific setup to compare the user’s achievable SNR of the above two systems. For a fair comparison, we constrain the total power consumption P^{\max} of the two systems as 2 W by setting $P_{BS-P}^{\max} = 2$ W for the passive RIS aided system and $P_{BS-A}^{\max} = P_A^{\max} = 1$ W for the active RIS aided system, respectively. Therefore, when $\sigma^2 = \sigma_v^2 = -70$ dBm and $\varrho_f^2 = \varrho_g^2 = -70$ dB, the required element number N for the passive RIS to outperform the active RIS will be 2.5×10^6 according to (7), which is impractical to realize with current technology. Conversely, for a more practical element number $N = 256$, according to (6) and (5), the SNR achieved by the passive RIS is $\gamma_{\text{passive}} \approx 9.0$ dB, while the SNR achieved by the active RIS is $\gamma_{\text{active}} \approx 49.0$ dB, which is about 10,000 times higher than γ_{passive} .

To show these results explicitly, we further plot the asymptotic SNR against the number of RIS elements N for both passive RISs and active RISs in Fig. 3, where N ranges from 10 to 1000 in Fig. 3 (a) and from 10^4 to 3×10^6 in Fig. 3 (b). From this figure we can observe that, when N ranges from 10 to 1000, the user’s achievable SNR of the active RIS aided system is about 40 dB higher than that of the passive RIS aided system. Only when $N = 2.5 \times 10^6$ can the performance gain achieved by the passive RIS be comparable to that achieved by the active RIS, which has agreed with our above analysis.

Remark 3: From the above comparisons we find that, although additional thermal noise is introduced by the active components, active RISs can still achieve an improved SNR. This is due to the fact that, the desired signals reflected by different active RIS elements can be coherently added with the same phase at the user, while the introduced noises cannot, which determines the positive influence of active RISs for capacity improvement. To support this insight, more simulation results will be present in later Section V.

IV. JOINT TRANSMIT BEAMFORMING AND REFLECT PRECODING DESIGN

To investigate the capacity gain enabled by the use of active RISs in typical wireless communication systems, in this section, the SISO case analyzed in Section III is extended to the more general MIMO case. Specifically, we first formulate the problem of sum-rate maximization for an active RIS aided MIMO system in Subsection IV-A. Then, the proposed joint transmit beamforming and reflect precoding algorithm to solve the problem is introduced in Subsection IV-B. Finally, the convergence and computational complexity of the proposed algorithm are discussed in IV-C.

A. Capacity Maximization Problem Formulation

According to the transmission model for multi-user MIMO in (4), the signal-to-interference-plus-noise ratio (SINR) at

user k can be derived as

$$\gamma_k = \frac{|\bar{\mathbf{h}}_k^H \mathbf{w}_k|^2}{\sum_{j=1, j \neq k}^K |\bar{\mathbf{h}}_k^H \mathbf{w}_j|^2 + \|\mathbf{f}_k^H \mathbf{P} \Theta\|^2 \sigma_v^2 + \sigma^2}, \quad (8)$$

wherein $\bar{\mathbf{h}}_k^H = \mathbf{h}_k^H + \mathbf{f}_k^H \mathbf{P} \Theta \mathbf{G} \in \mathbb{C}^{1 \times M}$ is the equivalent channel from the BS to user k , which takes both the direct link and the reflection link into account. Similarly, the transmit power at BS P_{BS} and reflect power at the active RIS P_{A} can be respectively derived as

$$P_{\text{BS}} = \sum_{k=1}^K \|\mathbf{w}_k\|^2, \quad (9a)$$

$$P_{\text{A}} = \sum_{k=1}^K \|\mathbf{P} \Theta \mathbf{G} \mathbf{w}_k\|^2 + \|\mathbf{P} \Theta\|^2 \sigma_v^2. \quad (9b)$$

Therefore, the original problem of sum-rate maximization, subject to the power constraints at the BS and the active RIS, can be formulated as follows:

$$\mathcal{P}_o : \max_{\mathbf{w}, \mathbf{P}, \Theta} R_{\text{sum}} = \sum_{k=1}^K \log_2(1 + \gamma_k), \quad (10a)$$

$$\text{s.t. } C_1 : \sum_{k=1}^K \|\mathbf{w}_k\|^2 \leq P_{\text{BS}}^{\text{max}}, \quad (10b)$$

$$C_2 : \sum_{k=1}^K \|\mathbf{P} \Theta \mathbf{G} \mathbf{w}_k\|^2 + \|\mathbf{P} \Theta\|^2 \sigma_v^2 \leq P_{\text{A}}^{\text{max}}, \quad (10c)$$

where $\mathbf{w} := [\mathbf{w}_1^T, \dots, \mathbf{w}_K^T]^T$ is the overall transmit beamforming vector for k users; C_1 and C_2 are the power constraints at the BS and active RIS, respectively.

We note that, due to the non-convexity and highly coupled variables in problem \mathcal{P}_o in (10), the joint design of \mathbf{w} , \mathbf{P} , and Θ is challenging. To efficiently solve this problem, we propose a joint beamforming and precoding algorithm based on alternating optimization and fractional programming, as illustrated in the next subsection.

B. Proposed joint beamforming and precoding algorithm

To solve the problem efficiently, we consider to simplify the problem at first. Note that, in problem \mathcal{P}_o in (10), \mathbf{P} and Θ always appear in product form. Therefore, \mathbf{P} and Θ can be merged as $\Psi = \mathbf{P} \Theta = \text{diag}(p_1 e^{j\theta_1}, \dots, p_N e^{j\theta_N}) \in \mathbb{C}^{N \times N}$. In this way, the optimizations of \mathbf{P} and Θ can be equivalently transformed to the optimization of Ψ , which we call RIS precoding matrix. Next, to deal with the non-convex sum-of-logarithms and fractions in (10), we exploit fractional programming [33] to decouple the variables in problem \mathcal{P}_o in (10), and then we obtain the following lemma.

Lemma 4 (Equivalent problem for sum-rate maximization): By introducing auxiliary variables $\rho := [\rho_1, \dots, \rho_K] \in$

Algorithm 1 Proposed joint transmit beamforming and reflect precoding algorithm

Input: Channels \mathbf{G} , \mathbf{h}_k , and \mathbf{f}_k , $\forall k \in \{1, \dots, K\}$.
Output: Optimized BS beamforming vector \mathbf{w} , amplification factor matrix of active RIS \mathbf{P} , phase shift matrix of active RIS Θ , and sum-rate R_{sum} .

- 1: Randomly initialize \mathbf{w} , \mathbf{P} and Θ ;
- 2: **while** no convergence of R_{sum} **do**
- 3: Update ρ by (13);
- 4: Update ϖ by (14);
- 5: Update \mathbf{w} by solving (16);
- 6: Update Ψ by solving (18);
- 7: Update R_{sum} by (10a);
- 8: **end while**
- 9: Obtain \mathbf{P} and Θ from Ψ ;
- 10: **return** Optimized \mathbf{w} , \mathbf{P} , Θ , and R_{sum} .

\mathbb{R}_+^K and $\varpi := [\varpi_1, \dots, \varpi_K] \in \mathbb{C}^K$, the original problem \mathcal{P}_o in (10) can be equivalently reformulated as follows

$$\begin{aligned} \mathcal{P}_1 : \max_{\mathbf{w}, \Psi, \rho, \varpi} R'_{\text{sum}} &= \sum_{k=1}^K \ln(1 + \rho_k) - \sum_{k=1}^K \rho_k + \\ &\quad \sum_{k=1}^K g_k(\mathbf{w}, \Psi, \rho_k, \varpi_k), \quad (11) \\ \text{s.t. } C_1 : \|\mathbf{w}\|^2 &\leq P_{\text{BS}}^{\text{max}}, \\ C_2 : \sum_{k=1}^K \|\Psi \mathbf{G} \mathbf{w}_k\|^2 &+ \|\Psi\|^2 \sigma_v^2 \leq P_{\text{A}}^{\text{max}}, \end{aligned}$$

where $g_k(\mathbf{w}, \Psi, \rho_k, \varpi_k)$ is defined as

$$\begin{aligned} g_k(\mathbf{w}, \Psi, \rho_k, \varpi_k) &= 2\sqrt{(1 + \rho_k)} \Re\{\varpi_k^* \bar{\mathbf{h}}_k^H \mathbf{w}_k\} - \\ &\quad |\varpi_k|^2 \left\{ \sum_{j=1}^K |\bar{\mathbf{h}}_k^H \mathbf{w}_j|^2 + \|\mathbf{f}_k^H \Psi\|^2 \sigma_v^2 + \sigma^2 \right\}. \quad (12) \end{aligned}$$

Proof: Constructive proof can be found in [33]. \blacksquare

According to the strong convergence of FP methods proved in [33], a locally optimal solution to (11) can be obtained by alternately optimizing the BS beamforming vector \mathbf{w} , RIS precoding matrix Ψ , auxiliary variables ρ and ϖ in (11), until R_{sum} converges. For clarity, we summarize the proposed joint beamforming and precoding algorithm in **Algorithm 1**, and the specific optimal solutions to variables \mathbf{w} , Ψ , ρ , and ϖ are given in the following four steps, respectively.

1) *Fix* $(\mathbf{w}, \Psi, \varpi)$ and then optimize ρ : While fixing the BS beamforming vector \mathbf{w} , RIS precoding matrix Ψ , and auxiliary variable ϖ , the optimal ρ can be obtained by solving $\frac{\partial R'_{\text{sum}}}{\partial \rho_k} = 0$ for (11) as

$$\rho_k^{\text{opt}} = \frac{\xi_k^2 + \xi_k \sqrt{\xi_k^2 + 4}}{2}, \quad \forall k \in \{1, \dots, K\}, \quad (13)$$

where $\xi_k = \Re\{\varpi_k^* \bar{\mathbf{h}}_k^H \mathbf{w}_k\}$.

2) *Fix* (\mathbf{w}, Ψ, ρ) and then optimize ϖ : While fixing the BS beamforming vector \mathbf{w} , RIS precoding matrix Ψ , and

auxiliary variable ρ , the optimal ϖ can be derived through solving $\frac{\partial R_{\text{sum}}^*}{\partial \varpi_k} = 0$ for (11), given by

$$\varpi_k^{\text{opt}} = \frac{\sqrt{(1 + \rho_k) \bar{\mathbf{h}}_k^H \mathbf{w}_k}}{\sum_{j=1}^K |\bar{\mathbf{h}}_k^H \mathbf{w}_j|^2 + \|\mathbf{f}_k^H \Psi\|^2 \sigma_v^2 + \sigma^2}, \quad (14)$$

$$\forall k \in \{1, \dots, K\}.$$

3) *Fix (Ψ, ρ, ϖ) and then optimize \mathbf{w}* : To simplify problem \mathcal{P}_1 in (11), we first define the following expressions:

$$\mathbf{b}_k^H = 2\sqrt{(1 + \rho_k) \varepsilon_k^* \bar{\mathbf{h}}_k^H}, \mathbf{b} = [\mathbf{b}_1^T, \mathbf{b}_2^T, \dots, \mathbf{b}_N^T]^T, \quad (15a)$$

$$\mathbf{A} = \mathbf{I}_K \otimes \sum_{k=1}^K |\varepsilon_k|^2 \bar{\mathbf{h}}_k \bar{\mathbf{h}}_k^H, \mathbf{\Xi} = \mathbf{I}_K \otimes (\mathbf{G}^H \Psi^H \Psi \mathbf{G}), \quad (15b)$$

$$P_m^{\text{max}} = P_A^{\text{max}} - \|\Psi\|^2 \sigma_v^2. \quad (15c)$$

Then, with fixed RIS precoding matrix Ψ and auxiliary variables ρ and ϖ , problem \mathcal{P}_1 in (11) can be reformulated as follows

$$\begin{aligned} \mathcal{P}_2: \quad & \max_{\mathbf{w}} \Re \{ \mathbf{b}^H \mathbf{w} \} - \mathbf{w}^H \mathbf{A} \mathbf{w}, \\ \text{s.t.} \quad & C_1: \|\mathbf{w}\|^2 \leq P_{\text{BS}}^{\text{max}}, \\ & C_2: \mathbf{w}^H \mathbf{\Xi} \mathbf{w} \leq P_m^{\text{max}}. \end{aligned} \quad (16)$$

Note that, \mathcal{P}_2 in (16) is a standard quadratic constraint quadratic programming (QCQP) problem. Thus, by adopting Lagrange multiplier method [34], the optimal solution \mathbf{w}^{opt} to \mathcal{P}_2 in (16) can be obtained by

$$\mathbf{w}^{\text{opt}} = (\mathbf{A} + \lambda_1 \mathbf{I}_{MK} + \lambda_2 \mathbf{\Xi})^{-1} \mathbf{b}, \quad (17)$$

where λ_1 and λ_2 are the Lagrange multipliers, which should be chosen such that the complementarity slackness conditions of the power constrains C_1 and C_2 are satisfied. The optimal Lagrange multipliers λ_1^{opt} and λ_2^{opt} can be obtained by adopting two-dimensional grid-search method [34].

4) *Fix $(\mathbf{w}, \rho, \varpi)$ and then optimize Ψ* : Define $\psi = [p_1 e^{j\theta_1}, \dots, p_N e^{j\theta_N}]^H$ as the vectorized RIS precoding matrix Ψ , i.e., $\text{diag}(\psi) := \Psi$. While fixing BS beamforming vector \mathbf{w} and auxiliary variables ρ and ϖ , problem \mathcal{P}_1 in (11) can be reformulated as

$$\begin{aligned} \mathcal{P}_3: \quad & \max_{\psi} \Re \{ \psi^H \mathbf{v} \} - \psi^H \Omega \psi, \\ \text{s.t.} \quad & C_2: \psi^H \Pi \psi \leq P_A^{\text{max}}, \end{aligned} \quad (18)$$

wherein

$$\begin{aligned} \mathbf{v} = 2 \sum_{k=1}^K \sqrt{(1 + \rho_k) \text{diag}(\varpi_k^* \mathbf{f}_k^H)} \mathbf{G} \mathbf{w}_k - \\ \sum_{k=1}^K |\varpi_k|^2 \text{diag}(\mathbf{f}_k^H) \mathbf{G} \sum_{j=1}^K \mathbf{w}_j \mathbf{w}_j^H \mathbf{h}_k, \end{aligned} \quad (19a)$$

$$\begin{aligned} \Omega = \sum_{k=1}^K |\varpi_k|^2 \text{diag}(\mathbf{f}_k^H) \text{diag}(\mathbf{f}_k) \sigma_v^2 + \\ \sum_{k=1}^K |\varpi_k|^2 \sum_{j=1}^K \text{diag}(\mathbf{f}_k^H) \mathbf{G} \mathbf{w}_j \mathbf{w}_j^H \mathbf{G}^H \text{diag}(\mathbf{f}_k), \end{aligned} \quad (19b)$$

$$\Pi = \sum_{k=1}^K \text{diag}(\mathbf{G} \mathbf{w}_k) (\text{diag}(\mathbf{G} \mathbf{w}_k))^H + \sigma_v^2 \mathbf{I}_N. \quad (19c)$$

Note that problem \mathcal{P}_3 in (18) is also a standard QCQP problem, thus the optimal solution ψ^{opt} can be obtained by adopting Lagrange multiplier method [34], written as

$$\psi^{\text{opt}} = (\Omega + \mu \Pi)^{-1} \mathbf{v}, \quad (20)$$

where μ is the Lagrange multiplier, which should be chosen such that the complementarity slackness conditions of the power constrain C_2 is satisfied. Similarly, the optimal Lagrange multiplier μ^{opt} can be obtained by adopting binary-search method [34].

C. Discussions of Convergence and Complexity

In this subsection, we analyze the convergence and the computational complexity of the proposed joint beamforming and precoding design algorithm, respectively.

1) *Convergence*: As an alternating optimization based algorithm, the proposed joint beamforming and precoding design has strict convergence. It is because that the iteration steps of the algorithm, i.e., the updates of auxiliary variable ρ in (13), auxiliary variable ϖ in (14), BS beamforming vector \mathbf{w} in (16), and RIS precoding matrix Ψ in (18), can be easily proved to be monotonous. Thanks to the strong convergence of FP methods [33], the proposed joint beamforming and precoding algorithm can be ensured to converge to a local optimal solution after several iterations.

2) *Computational complexity*: The overall computational complexity of the proposed algorithm is mainly introduced by the updates of the four variable ρ , ϖ , \mathbf{w} , and Ψ , as shown in (13), (14), (16), and (18), respectively. Let I_a denote the search numbers required by the grid searching for optimal Lagrange multipliers λ_1^{opt} and λ_2^{opt} , and let I_p denote that required by the binary searching for optimal Lagrange multiplier μ^{opt} . Then, the computational complexities of updating ρ , ϖ , \mathbf{w} , and Ψ can be derived as $\mathcal{O}(KM)$, $\mathcal{O}(K^2M + KN)$, $\mathcal{O}(I_a K^3 M^3)$, and $\mathcal{O}(I_p N^3)$, respectively. Let I_o denote the required iteration number for global convergence. Thus, the overall computational complexity for the proposed joint beamforming and precoding algorithm can be approximated by $\mathcal{O}(I_o (I_a K^3 M^3 + I_p N^3))$, which is acceptable for most computing devices.

V. VALIDATION RESULTS

In this section, for validating the developed signal model (2), we first present the experimental results based on a fabricated active RIS element in Subsection V-A. Then, simulation results are provided to evaluate the performance of an active RIS aided MIMO system in Subsection V-B. Finally, the impact of key parameters on system performances is discussed in Subsection V-C.

A. Validation Results for Signal Model

To validate the developed signal model (2), we designed and fabricated an active RIS element with integrated reflection-type amplifier for experimental measurements² in [35]. Note

²In October 2019, we start to design an active RIS element integrating a reflection-type amplifier. Then, the fabrication of this active RIS element was finished in August 2020. Subsequently, we set out to establish an experimental environment for the signal measurements on this element, and all measurements were completed in February 2021.

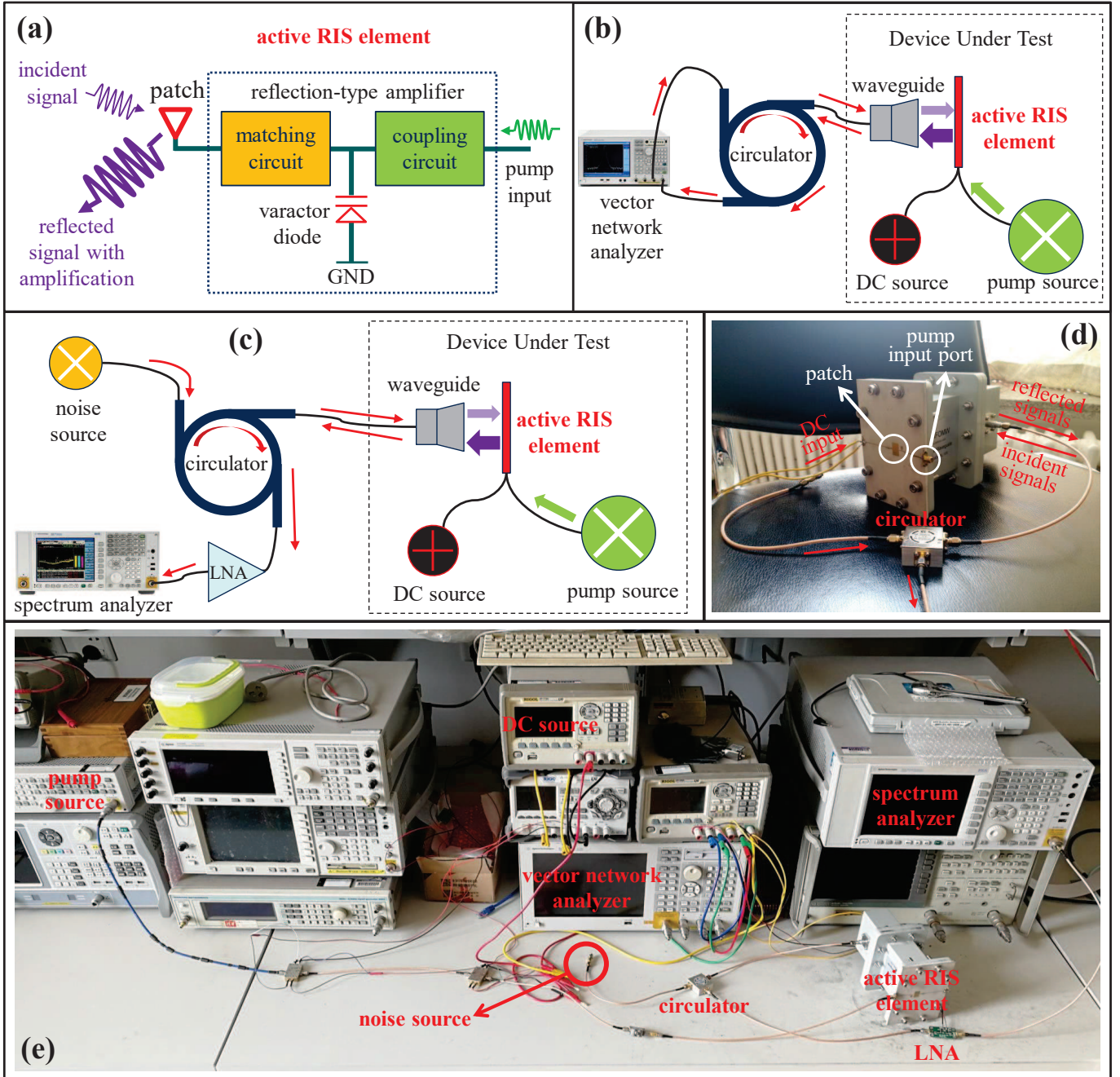


Fig. 4. The experimental devices and environment for validating the developed signal model (2) of the proposed active RIS.

that this design can be directly extended to the large-array case. Particularly, since the phase-shifting ability of RISs has been widely verified [18], we focus on studying the reflection gain and the noise introduced by an active RIS. Thus, the validation of signal model (2) is equivalent to validating

$$P_y = \underbrace{GP_x}_{\text{Desired-signal power}} + \underbrace{G\sigma_v^2 + \sigma_s^2}_{\text{noise power}}, \quad (21)$$

where P_y is the power of the signals reflected by the active RIS element; P_x is the power of the incident signal; $G := p^2$ is the reflection gain of the active RIS element; $G\sigma_v^2$ and σ_s^2 are the power of dynamic noise and static noise introduced at the active RIS element, respectively.

1) Platform illustration: To validate the model (21), we first establish the hardware platform for experimental measurements as shown in Fig. 4. Specifically, the detailed illustration of this platform is provided as follows.

- Fig. 4 (a) illustrates the structure of the fabricated active RIS element operating at a frequency of 2.36 GHz [35]. A pump input is used to supply the additional power for active RIS element. The incident signal and the pump input are coupled in a varactor-diode-based reflection-type amplifier to generate the reflected signal with amplification.
- Fig. 4 (b) illustrates the system used for measuring the reflection gain G of the active RIS element. A direct-

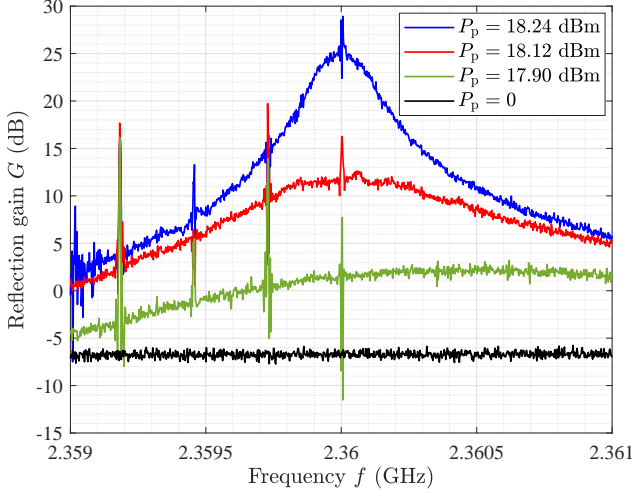


Fig. 5. Experimental measurement result for reflection gain G against signal frequency f .

current (DC) source is used to provide a bias voltage of 7.25 V for driving the active RIS element, and a controllable pump source is used to reconfigure the reflection gain G . A circulator is used to separate the incident signal and the reflected signal, and the reflection gain is directly measured by a vector network analyzer.

- Fig. 4 (c) illustrates the system for measuring the noises introduced at the active RIS element, where a spectrum analyzer is used to measure the noise power. The noise source is a 50 Ω impedance, which aims to simulate a natural input noise of -174 dBm/Hz at each patch. The reflected signal is amplified by a low-noise amplifier (LNA) so that the spectrum analyzer can detect it.
- Fig. 4 (d) shows a photo of the fabricated active RIS element under test, which is connected by a waveguide for incident/reflected signal exchanges.
- Fig. 4 (e) is a photo of the experimental environment with the required equipment for device driving and signal measurement.

2) *Reflection gain measurement*: Using the measurement system for the reflection gain depicted in Fig. 4 (b), we first investigate the reflection gain G of the active RIS element. Note that, the reflection gain G can be reconfigured by the input power of the pump source P_p . By setting the input power of the vector network analyzer as $P_x = -50$ dBm, the reflection gain G as a function of the signal frequency can be directly measured via the vector network analyzer. Then, in Fig. 5, we show the measurement results for the reflection gain G as a function of the signal frequency f and for different power of the pump source P_p . We can observe that, the active RIS element can achieve a reflection gain G of more than 25 dB, when $P_p = 18.24$ dBm, which confirms the significant reflection gains enabled by active RISs. On the other hand, when $P_p = 0$, we can observe that G falls to -6 dB, which is lower than the expected 0 dB. This loss is mainly caused by the inherent power losses of the circulator and transmission lines used for measurement.

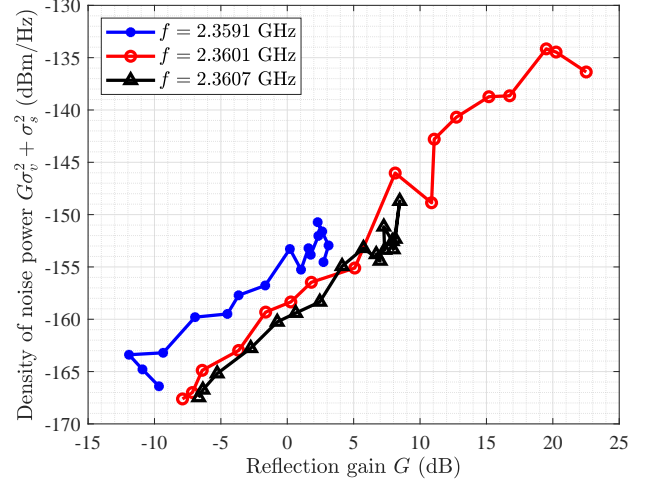


Fig. 6. Experimental measurement result for density of noise power $G\sigma_v^2 + \sigma_s^2$ against reflection gain G .

3) *Noise power measurement*: We further study the noise power introduced by the active RIS element, i.e., $G\sigma_v^2 + \sigma_s^2$ in (21), where $G\sigma_v^2$ and σ_s^2 are the power of dynamic noise and static noise introduced at the active RIS element, respectively. Using the noise measurement system in Fig. 4 (c), we show the measurement results for the spectral density of noise power $G\sigma_v^2 + \sigma_s^2$ as a function of G for different operating frequencies in Fig. 6. We can observe that the noise power increases nearly linearly with G , which verifies the noise model $G\sigma_v^2 + \sigma_s^2$ in (21). Particularly, for $f = 2.3601$ GHz, the spectral density of σ_s^2 is about -174 dBm/Hz, while that of σ_v^2 is about -160 dBm/Hz, which is about 15 dB higher. The reason for this is that the input noise is amplified by the noise factor [23], and additional noises are also introduced by the other active components in our measurements, such as the leakage noise from the DC source.

B. Simulation Results for Joint Beamforming and Precoding Design

To evaluate the performance of the proposed active RIS in typical wireless systems, in this subsection, we present simulation results for passive RIS and active RIS aided MIMO systems, respectively.

1) *Simulation setup*: For the simulation setup, we consider an active RIS aided MIMO system as shown in Fig. 7. Particularly, we consider two scenarios with different channel conditions as shown in Fig. 7 (a) and (b), respectively. For both scenarios, the BS-RIS-user reflection link is LoS, while the BS-user direct link is blocked in scenario 1 and LoS in scenario 2. As common settings, the BS and the active/passive RIS are located at (0, -40 m) and (200 m, 30 m), respectively. The four users are randomly located in a circle with a radius of 5 m from the center ($L, 0$). The operating frequency is set as $f = 5$ GHz, and the antenna/element spacing is set as half wavelength. Unless specified, the numbers of BS antennas and RIS elements are set as $M = 4$ and $N = 256$, respectively. The noise power is set as $\sigma^2 = \sigma_v^2 = -70$ dBm. The free-

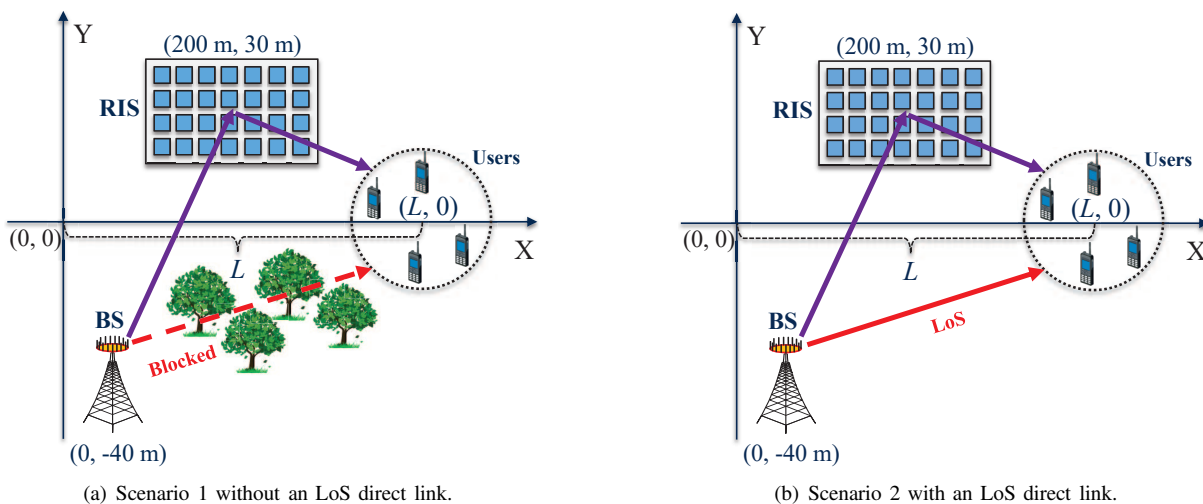


Fig. 7. Two simulation scenarios with different channel conditions, where a BS aided by an active RIS serves four users.

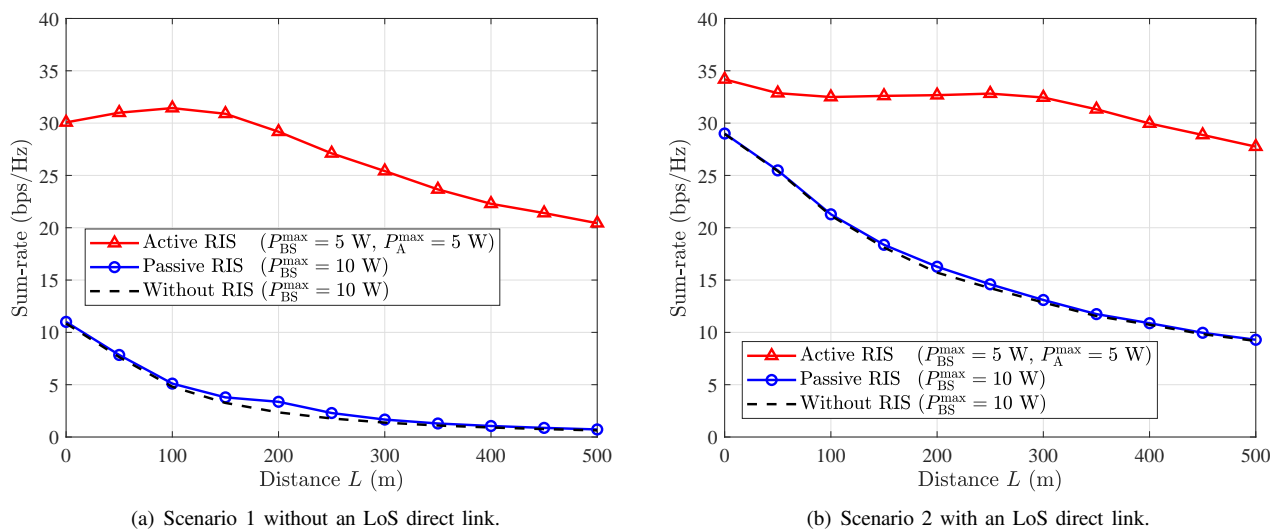


Fig. 8. Simulation results for the sum-rate against distance L in an RIS-aided MIMO system.

space model [17] with Rayleigh small-scale fading is used to generate all channels. To characterize the case when the direct link is blocked, we assume that the channel gain of the blocked link is 1% of that of the unobstructed line-of-sight (LoS). [9]. The other parameter settings are summarized in Table I. For fair comparison, we constrain the total power consumption $P^{\max} := P_{\text{BS}}^{\max} + P_{\text{A}}^{\max}$ to 10 W by setting $P_{\text{BS}}^{\max} = P_{\text{A}}^{\max} = 5$ W for the active RIS aided system and $P_{\text{BS}}^{\max} = 10$ W for the benchmark systems. For the active RIS, the proposed **Algorithm 1** is employed to achieve joint beamforming and precoding design, while for the passive RIS, an existing joint beamforming and precoding algorithm in [21] is used.

2) *Simulation results*: In Fig. 8 (a) and (b), we plot the sum-rate against distance L in the two scenarios, where the direct link is LoS and blocked, respectively. From these results, we have two observations. Firstly, in scenario 1 without an LoS direct link, the passive RIS can indeed achieve a performance improvement, while the active RIS achieves a much higher

sum-rate gain. Secondly, in scenario 2 with an LoS direct link, the passive RIS achieves only a negligible sum-rate gain, while the active RIS can still realize a noticeable sum-rate gain. For example, when $L = 200$ m, the capacities without RIS, with passive RIS, and with active RIS in scenario 1 are 2.35 bps/Hz, 3.37 bps/Hz, and 29.18 bps/Hz respectively, while in scenario 2, these values are 15.71 bps/Hz, 16.27 bps/Hz, and 32.67 bps/Hz, respectively. At this position, the passive RIS provides a 43% gain in scenario 1 and a negligible 3% gain in scenario 2. By contrast, active RIS can achieve noticeable sum-rate gains of 1142% in scenario 1 and 108% in scenario 2, which are much higher than those achieved by the passive RIS in the corresponding scenarios. These results demonstrate that, compared with the existing passive RIS, the proposed active RIS can overcome the “multiplicative fading” effect and achieve noticeable sum-rate gains in both communication scenarios.

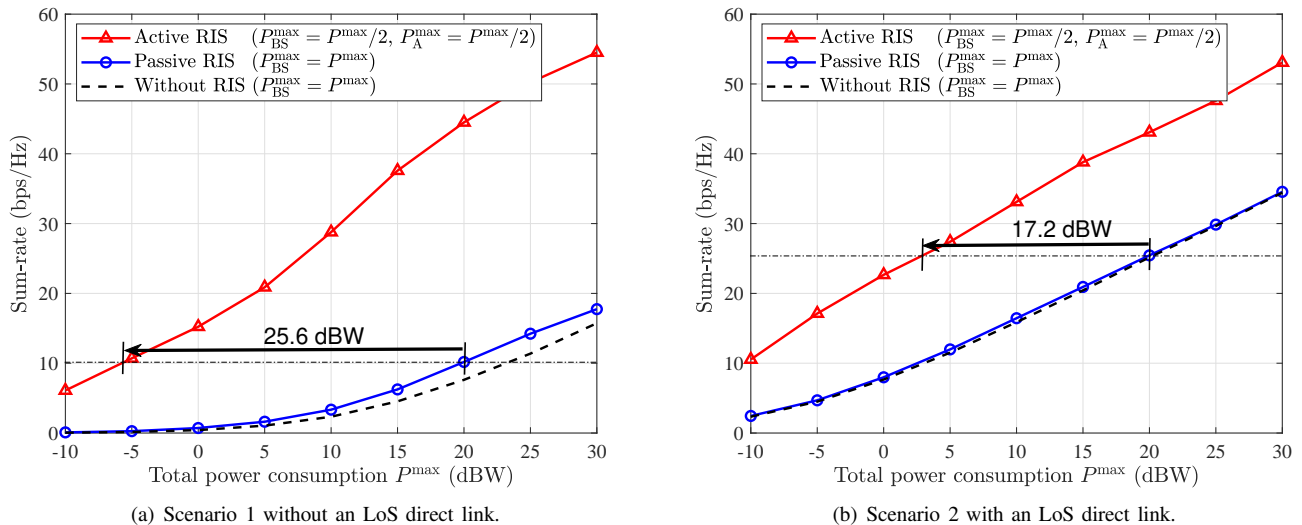


Fig. 9. Simulation results for the sum-rate against the total power consumption P^{\max} in an RIS-aided MIMO system.

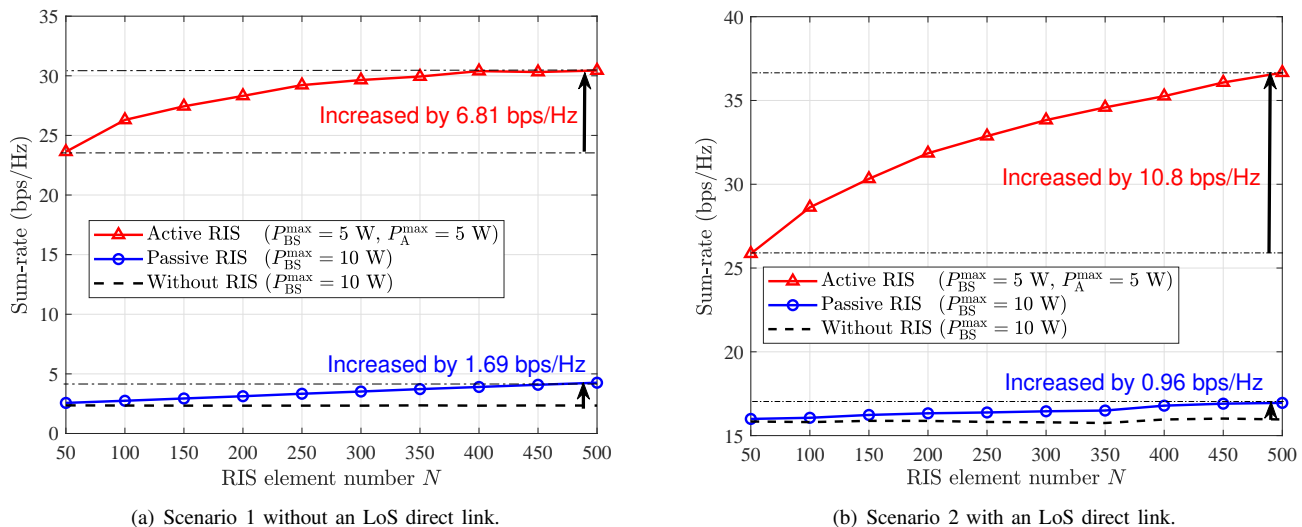


Fig. 10. Simulation results for the sum-rate against the RIS element number N in an RIS-aided MIMO system.

C. The Impact of Key Parameters on System Performance

To observe more insights of the active RIS aided communication system, in this subsection, we study the impact of key parameters, including the total power consumption P^{\max} and the number of RIS elements N , on the sum-rate performance.

1) *Sum-rate against total power consumption P^{\max}* : Using the same simulation setup in Subsection V-B and fixing the distance as $L = 200$ m, we plot the users' sum-rate against the total transmit power P^{\max} in Fig. 9. For scheme "Active RIS", we assume the total power consumption P^{\max} is equally allocated to the BS and the active RIS for a fair comparison. From these two subfigures we observe that, the passive RIS only achieves visible performance gains in scenario 1 where the direct link is LoS, while in scenario with an LoS direct link, the passive RIS achieves negligible sum-rate gain. By contrast, in both scenarios, the active RIS realizes a high per-

formance gain. Particularly, we note that, to achieve the same performance as the passive RIS aided system, the required power consumption for the active RIS aided system is much lower. For example, when the total power consumption of the passive RIS aided system is 20 dBW, to achieve the same capacity, the active RIS aided system only consumes -5.6 dBW in scenario 1 and 2.8 dBW in scenario 2, which saves the total power of 25.6 dBW and 17.2 dBW, respectively. The reason for this result is that, for scheme "Passive RIS", the total power is only allocated to the BS, thus all transmit power suffers path loss twice. However, for scheme "Active RIS", half of the transmit power is allocated to the active RIS, and this part of power only suffers path loss once. It implies that, to achieve the same performance, the total power required by the active RIS aided system is lower than that of the passive RIS aided system, thus the proposed active RIS is promising to reduce the required transmit power in communication systems.

2) *Sum-rate against the number of RIS elements N* : Under the same setup, we plot the users' sum-rate against the RIS element number N in Fig. 10. From these two subfigures, we can observe that, as the RIS element number N increases, both the passive RIS and the active RIS can achieve higher sum-rate gain, while the performance improvement of the active RIS aided system is greater than that of the passive RIS aided system. For example, when the number of RIS elements N increases from 50 to 500, the sum-rate of passive RIS aided system increases from 2.57 bps/Hz to 4.26 bps/Hz in scenario 1 and from 15.99 bps/Hz to 16.95 bps/Hz in scenario 2, corresponding to the increases of 1.69 bps/Hz and 0.96 bps/Hz, respectively. By contrast, the sum-rate of active RIS aided system increases from 23.63 bps/Hz to 30.44 bps/Hz in scenario 1 (increased by 6.81 bps/Hz) and from 25.86 bps/Hz to 36.66 bps/Hz in scenario 2 (increased by 10.8 bps/Hz), which rises much faster than that of the passive RIS aided system. It indicates that, when the element number N is not too large (such as millions of elements), compared with the passive RIS, increasing the element number of the active RIS is more efficient to improve the system capacity, which agrees with the performance analysis in Section III.

VI. CONCLUSIONS AND FUTURE WORKS

In this paper, we tried to overcome the fundamental limitation of the ‘‘multiplicative fading’’ effect by proposing a new architecture of active RISs. Our developed signal model for active RISs characterized the amplification of incident signals and incorporates the non-negligible thermal noise introduced by the active elements, which was validated by experimental measurements. Asymptotic analysis revealed the high SNR gain enabled by active RISs, and a joint beamforming and precoding algorithm was proposed to maximize the sum-rate in an active RIS aided MIMO system. Simulations results have shown that, the proposed active RISs achieves a 108% sum-rate gain in a typical scenario thus it overcomes the ‘‘multiplicative fading’’ effect. Our works can serve as guidelines for many possible works on active RISs in the future, such as hardware design [22], prototype development [7], channel estimation [20], energy efficiency analysis [10], etc.

APPENDIX A PROOF OF LEMMA 2

Since the considered scenario is an active RIS aided SISO system without direct link, we first redefine $\mathbf{G} := \mathbf{g} = [g_1, \dots, g_N]^T$, $\mathbf{f}_k := \mathbf{f} = [f_1, \dots, f_N]^T$, and $\mathbf{w}_k := w$ to simplify the expressions. Thus, the downlink transmission model in (4) can be rewritten as

$$r = \underbrace{p\mathbf{f}^H\Theta\mathbf{g}}_{\text{Reflection link}} ws + \underbrace{p\mathbf{f}^H\Theta\mathbf{v}}_{\text{Noise introduced by active RIS}} + \underbrace{z}_{\text{Noise introduced at user}}, \quad (22)$$

where $r \in \mathbb{C}$ is the signal received by the user. Based on the transmission model (22), the transmit power at BS P_{BS} and the reflect power at the active RIS P_A can be respectively derived as

$$P_{\text{BS}} = |w|^2, \quad (23a)$$

$$P_A = p^2\|\Theta\mathbf{g}w\|^2 + p^2N\sigma_v^2. \quad (23b)$$

Thus, the maximization of the user's SNR γ , subject to the power constraints at the BS and the active RIS, can be formulated as follows:

$$\begin{aligned} \max_{w, p, \Theta} \quad & \gamma = \frac{|p\mathbf{f}^H\Theta\mathbf{g}w|^2}{p^2\|\mathbf{f}^H\Theta\|^2\sigma_v^2 + \sigma^2}, \\ \text{s.t.} \quad & C_1 : |w|^2 \leq P_{\text{BS}}^{\max}, \\ & C_2 : p^2\|\Theta\mathbf{g}w\|^2 + p^2N\sigma_v^2 \leq P_A^{\max}, \end{aligned} \quad (24)$$

where P_{BS}^{\max} and P_A^{\max} denote the maximum transmit power and reflect power at the BS and the active RIS, respectively.

Since problem (24) is convex, the optimal solution of problem (24) can be obtained by the Lagrange multiplier method, given by

$$w^{\text{opt}} = \sqrt{P_{\text{BS}}^{\max}}, \quad (25a)$$

$$\theta_n^{\text{opt}} = \angle f_n - \angle g_n, \quad \forall n \in \{1, \dots, N\}, \quad (25b)$$

$$p^{\text{opt}} = \sqrt{\frac{P_A^{\max}}{P_{\text{BS}}^{\max} \sum_{n=1}^N |g_n|^2 + N\sigma_v^2}}. \quad (25c)$$

By substituting (25) into (24), the user's maximum achievable SNR for active RISs can be obtained as

$$\gamma_{\text{active}} = \frac{P_{\text{BS}}^{\max} P_A^{\max} \left| \sum_{n=1}^N |f_n| |g_n| \right|^2}{P_A^{\max} \sigma_v^2 \sum_{n=1}^N |f_n|^2 + \sigma^2 \left(P_{\text{BS}}^{\max} \sum_{n=1}^N |g_n|^2 + N\sigma_v^2 \right)}. \quad (26)$$

Note that, $\mathbf{f} \sim \mathcal{CN}(\mathbf{0}_N, \rho_f^2 \mathbf{I}_N)$ and $\mathbf{g} \sim \mathcal{CN}(\mathbf{0}_N, \rho_g^2 \mathbf{I}_N)$. By letting $N \rightarrow \infty$ in (26), according to the law of large numbers, we have

$$\sum_{n=1}^N |f_n| |g_n| \rightarrow N \frac{\pi \rho_f \rho_g}{4}, \quad (27a)$$

$$\sum_{n=1}^N |g_n|^2 \rightarrow N \rho_g^2, \quad (27b)$$

$$\sum_{n=1}^N |f_n|^2 \rightarrow N \rho_f^2. \quad (27c)$$

After substituting (27) into (26), we can derive the asymptotic SNR for active RISs as (6), which completes the proof.

APPENDIX B PROOF OF LEMMA 3

According to the related analysis in [32] and Appendix A, the user's achievable SNR for an SISO system aided by a passive RIS and that aided by an active RIS can be respectively written as

$$\gamma_{\text{passive}} = \frac{P_{\text{BS-P}}^{\max} \left| \sum_{n=1}^N |f_n| |g_n| \right|^2}{\sigma^2}, \quad (28a)$$

$$\gamma_{\text{active}} = \frac{P_{\text{BS-A}}^{\max} P_A^{\max} \left| \sum_{n=1}^N |f_n| |g_n| \right|^2}{P_A^{\max} \sigma_v^2 \sum_{n=1}^N |f_n|^2 + \sigma^2 \left(P_{\text{BS-A}}^{\max} \sum_{n=1}^N |g_n|^2 + N\sigma_v^2 \right)}, \quad (28b)$$

where $P_{\text{BS-A}}^{\max}$ denotes the maximum BS transmit power in the active RIS aided system and $P_{\text{BS-P}}^{\max}$ denotes that in the passive

$$\begin{aligned}
N &\geq \frac{P_{\text{BS-A}}^{\text{max}}}{P_{\text{BS-P}}^{\text{max}}} \frac{P_{\text{A}}^{\text{max}} \sigma^2}{P_{\text{A}}^{\text{max}} \sigma_v^2 \frac{1}{N} \sum_{n=1}^N |f_n|^2 + \sigma^2 \left(P_{\text{BS}}^{\text{max}} \frac{1}{N} \sum_{n=1}^N |g_n|^2 + \sigma_v^2 \right)} \\
&\approx \frac{P_{\text{BS-A}}^{\text{max}}}{P_{\text{BS-P}}^{\text{max}}} \frac{P_{\text{A}}^{\text{max}} \sigma^2}{\left(P_{\text{A}}^{\text{max}} \sigma_v^2 \varrho_f^2 + P_{\text{BS-A}}^{\text{max}} \sigma^2 \varrho_g^2 + \sigma^2 \sigma_v^2 \right)}.
\end{aligned} \tag{29}$$

RIS aided system. By solving $\gamma_{\text{passive}} \geq \gamma_{\text{active}}$ according to (28), we obtain (29) at the top of this page.

We note that $\mathbf{f} \sim \mathcal{CN}(\mathbf{0}_N, \varrho_f^2 \mathbf{I}_N)$ and $\mathbf{g} \sim \mathcal{CN}(\mathbf{0}_N, \varrho_g^2 \mathbf{I}_N)$. Since the number of RIS elements N is usually large, the components $\frac{1}{N} \sum_{n=1}^N |f_n|^2$ and $\frac{1}{N} \sum_{n=1}^N |g_n|^2$ in (29) can be reasonably approximated by ϱ_f^2 and ϱ_g^2 , which completes the proof.

REFERENCES

- [1] L. Zhang, X. Q. Chen, S. Liu, Q. Zhang, J. Zhao, J. Y. Dai, G. D. Bai, X. Wan, Q. Cheng, G. Castaldi, V. Galdi, and T. J. Cui, "Space-time-coding digital metasurfaces," *Nat. Commun.*, vol. 9, no. 4338, Oct. 2018.
- [2] X. Ni, A. V. Kildishev, and V. M. Shalaev, "Metasurface holograms for visible light," *Nat. Commun.*, vol. 4, no. 2807, Nov. 2013.
- [3] H. Ren, "A light-programmable metasurface," *Nat. Elect.*, vol. 3, pp. 137–138, Mar. 2020.
- [4] S. Venkatesh, X. Lu, H. Saeidi, and K. Sengupta, "A high-speed programmable and scalable terahertz holographic metasurface based on tiled CMOS chips," *Nat. Elect.*, vol. 3, pp. 785–793, Dec. 2020.
- [5] M. Di Renzo, A. Zappone, M. Debbah, M. S. Alouini, C. Yuen, J. de Rosny, and S. Tretyakov, "Smart radio environments empowered by reconfigurable intelligent surfaces: How it works, state of research, and the road ahead," *IEEE J. Sel. Areas Commun.*, vol. 38, no. 11, pp. 2450–2525, Nov. 2020.
- [6] E. Basar, M. Di Renzo, J. De Rosny, M. Debbah, M. Alouini, and R. Zhang, "Wireless communications through reconfigurable intelligent surfaces," *IEEE Access*, vol. 7, pp. 116 753–116 773, Aug. 2019.
- [7] L. Dai, B. Wang, M. Wang, X. Yang, J. Tan, S. Bi, S. Xu, F. Yang, Z. Chen, M. Di Renzo, C. B. Chae, and L. Hanzo, "Reconfigurable intelligent surface-based wireless communications: Antenna design, prototyping, and experimental results," *IEEE Access*, vol. 8, pp. 45 913–45 923, Mar. 2020.
- [8] C. Huang, R. Mo, and C. Yuen, "Reconfigurable intelligent surface assisted multiuser MISO systems exploiting deep reinforcement learning," *IEEE J. Sel. Areas Commun.*, vol. 38, no. 8, pp. 1839–1850, Aug. 2020.
- [9] P. Wang, J. Fang, X. Yuan, Z. Chen, and H. Li, "Intelligent reflecting surface-assisted millimeter wave communications: Joint active and passive precoding design," *IEEE Trans. Veh. Technol.*, vol. 69, no. 12, pp. 14 960–14 973, Dec. 2020.
- [10] C. Huang, A. Zappone, G. C. Alexandropoulos, M. Debbah, and C. Yuen, "Reconfigurable intelligent surfaces for energy efficiency in wireless communication," *IEEE Trans. Wireless Commun.*, vol. 18, no. 8, pp. 4157–4170, Aug. 2019.
- [11] H. Zhao, Y. Shuang, M. Wei, T. J. Cui, P. Hougue, and L. Li, "Metasurface-assisted massive backscatter wireless communication with commodity Wi-Fi signals," *Nat. Commun.*, vol. 11, no. 3926, Aug. 2020.
- [12] M. Faraji-Dana, E. Arbabi, A. Arbabi, S. M. Kamali, H. Kwon, and A. Faraon, "Compact folded metasurface spectrometer," *Nat. Commun.*, vol. 9, no. 4196, Oct. 2013.
- [13] J. Park, B. G. Jeong, S. I. Kim, D. Lee, J. Kim, C. Shin, C. B. Lee, T. Otsuka, J. Kyoung, S. Kim, K. Yang, Y. Park, J. Lee, I. Hwang, J. Jang, S. H. Song, M. L. Brongersma, K. Ha, S. Hwang, H. Choo, and B. L. Choi, "All-solid-state spatial light modulator with independent phase and amplitude control for three-dimensional LiDAR applications," *Nat. Nanotechnol.*, vol. 16, p. 69–76, Oct. 2020.
- [14] W. Zhao, G. Wang, S. Atapattu, T. A. Tsiftsis, and C. Tellambura, "Is backscatter link stronger than direct link in reconfigurable intelligent surface-assisted system?" *IEEE Commun. Lett.*, vol. 24, no. 6, pp. 1342–1346, Jun. 2020.
- [15] T. Hou, Y. Liu, Z. Song, X. Sun, and Y. Chen, "MIMO-NOMA networks relying on reconfigurable intelligent surface: A signal cancellation-based design," *IEEE Trans. Commun.*, vol. 68, no. 11, pp. 6932–6944, Nov. 2020.
- [16] Z. Zhang and L. Dai, "A joint precoding framework for wideband reconfigurable intelligent surface-aided cell-free network," *IEEE Trans. Signal Process.*, vol. 69, pp. 4085–4101, Aug. 2021.
- [17] M. Najafi, V. Jamali, R. Schober, and H. V. Poor, "Physics-based modeling and scalable optimization of large intelligent reflecting surfaces," *IEEE Trans. Commun.*, vol. 69, no. 4, pp. 2673–2691, Apr. 2021.
- [18] H. Yang, F. Yang, X. Cao, S. Xu, J. Gao, X. Chen, M. Li, and T. Li, "A 1600-element dual-frequency electronically reconfigurable reflectarray at x/ku-band," *IEEE Trans. Antennas Propag.*, vol. 65, no. 6, pp. 3024–3032, Jun. 2017.
- [19] D. Headland, T. Niu, E. Carrasco, D. Abbott, S. Sriram, M. Bhaskaran, C. Fumeaux, and W. Withayachumnankul, "Terahertz reflectarrays and nonuniform metasurfaces," *IEEE J. Sel. Topics Quantum Electron.*, vol. 23, no. 4, pp. 1–18, Aug. 2017.
- [20] C. Hu, L. Dai, S. Han, and X. Wang, "Two-timescale channel estimation for reconfigurable intelligent surface aided wireless communications," *IEEE Trans. Commun.*, vol. 69, no. 11, pp. 7736–7747, Nov. 2021.
- [21] C. Pan, H. Ren, K. Wang, W. Xu, M. Elkashlan, A. Nallanathan, and L. Hanzo, "Multicell MIMO communications relying on intelligent reflecting surfaces," *IEEE Trans. Wireless Commun.*, vol. 19, no. 8, pp. 5218–5233, Aug. 2020.
- [22] J. Lončar, Z. Šipuš, and S. Hrabar, "Ultrathin active polarization-selective metasurface at X-band frequencies," *Physical Review B*, vol. 100, no. 7, p. 075131, Oct. 2019.
- [23] J. Bousquet, S. Magierowski, and G. G. Messier, "A 4-GHz active scatterer in 130-nm CMOS for phase sweep amplify-and-forward," *IEEE Trans. Circuits Syst. I*, vol. 59, no. 3, pp. 529–540, Mar. 2012.
- [24] K. K. Kishor and S. V. Hum, "An amplifying reconfigurable reflectarray antenna," *IEEE Trans. Antennas Propag.*, vol. 60, no. 1, pp. 197–205, Jan. 2012.
- [25] X. Mu, Y. Liu, L. Guo, J. Lin, and R. Schober, "Simultaneously transmitting and reflecting (STAR) RIS aided wireless communications," *IEEE Trans. Wireless Commun.*, Oct. 2021.
- [26] Y. Liu, X. Mu, J. Xu, R. Schober, Y. Hao, H. V. Poor, and L. Hanzo, "STAR: Simultaneous transmission and reflection for 360° coverage by intelligent surfaces," arXiv preprint arXiv:2103.09104, Mar. 2021.
- [27] S. Zeng, H. Zhang, B. Di, Y. Tan, Z. Han, H. V. Poor, and L. Song, "Reconfigurable intelligent surfaces in 6G: Reflective, transmissive, or both?" *IEEE Commun. Lett.*, vol. 25, no. 6, pp. 2063–2067, Jun. 2021.
- [28] J. He, N. T. Nguyen, R. Schroeder, V. Tapio, J. Kokkonen, and M. Juntti, "Channel estimation and hybrid architectures for ris-assisted communications," in *Proc. 2021 Joint European Conf. Netw. Commun. 6G Summit (EuCNC/6G Summit'21)*, Jun. 2021, pp. 60–65.
- [29] N. T. Nguyen, Q.-D. Vu, K. Lee, and M. Juntti, "Hybrid relay-reflecting intelligent surface-assisted wireless communication," arXiv preprint arXiv:2103.03900, Mar. 2021.
- [30] E. Basar, "Transmission through large intelligent surfaces: A new frontier in wireless communications," in *Proc. European Conf. Netw. Commun. (EuCNC'19)*, Jun. 2019, pp. 1–6.
- [31] K. Ntontin, J. Song, and M. D. Renzo, "Multi-antenna relaying and reconfigurable intelligent surfaces: End-to-end SNR and achievable rate," arXiv preprint arXiv:1908.07967, Aug. 2019.
- [32] Q. Wu and R. Zhang, "Intelligent reflecting surface enhanced wireless network via joint active and passive beamforming," *IEEE Trans. Wireless Commun.*, vol. 18, no. 11, pp. 5394–5409, Nov. 2019.
- [33] K. Shen and W. Yu, "Fractional programming for communication systems—part I: Power control and beamforming," *IEEE Trans. Signal Process.*, vol. 66, no. 10, pp. 2616–2630, May 2018.
- [34] S. Boyd, N. Parikh, E. Chu, B. Peleato, and J. Eckstein, "Distributed optimization and statistical learning via the alternating direction method of multipliers," Nov. 2014, [Online] Available: https://stanford.edu/~boyd/papers/pdf/admm_distr_stats.pdf.
- [35] X. Chen and F. Yang, "Nonlinear electromagnetic surfaces: Theory, design and application," *Master Thesis in Tsinghua University*, May 2020, [Online] Available: <http://etds.lib.tsinghua.edu.cn/Thesis>.